
PHYSICAL SIMILARITY OF FLUID FLOW IN BIMODAL POROUS MEDIA: PART 1 – BASIC MODEL AND SOLUTION CHARACTERISTICS

Yuhe Wang^{1,2,*,**} and Yating Wang³

¹ National & Local Joint Engineering Laboratory for Big Data Analysis and Computing Technology,
Beijing 100190, China

² Institute for Scientific Computation, Texas A&M University, College Station, Texas 77843, USA

³ School of Mathematics and Statistics, Xi'an Jiaotong University, Xi'an, Shaanxi 710049, China

August 28, 2024

Abstract. Fluid flow through bimodal porous media, characterized by a distinct separation in pore size distribution, is critical in various scientific and engineering applications, including groundwater management, oil and gas production, and carbon sequestration. This note delves into the physical similarity of fluid flow within such media, bridging the gap between microscale phenomena and macroscale observations. We present a representative mathematical model that conceptualizes bimodal porous media as a double-continuum system, distinguishing between macroporous and microporous regions. The model captures the complex interactions between these regions, particularly focusing on the challenges of modeling fluid flow when there is significant disparity in pore sizes. By employing a heuristic approach grounded in pore-scale tomography, we derive governing equations that describe fluid flow and analyze the solution characteristics. The results reveal unique features of the fluid flow in bimodal systems, such as the occurrence of boundary discontinuities and the delayed transient response, which are not observed in conventional porous media. This work provides ground for further studies in bimodal porous media, offering insights that could enhance predictive modeling and optimization in various applications concerning porous media with similar bimodal pore size distributions.

Keywords. Bimodal porous media, Fluid flow through porous media, Microscale, Macroscale, Physical similarity, Double-continuum model

Background. Sharp bimodal pore size distributions are frequently observed in both naturally occurring and artificially fabricated porous media, including natural rocks [1, 2, 3, 4], zeolites [5], photocatalytic TiO₂ [6], and porous carbons [7]. The fluid flow processes within these bimodal porous media are of considerable scientific and engineering importance. A typical sharp bimodal pore size distribution is characterized by two distinctly separated peaks, as illustrated in **Figure 1**. The magnitude difference between the two peak pore radii can be the order of two or more, as is often the case for carbonate rocks [1, 2, 8]. Bimodal carbonates, commonly referred to as microporous carbonates, consist of macropores with radii in the range of hundreds of microns and micropores with radii of a few microns. Understanding the fluid flow through microporous carbonates is fundamental to several critical applications, including groundwater management [9, 10], oil and gas production from carbonate reservoirs [11, 12, 13], and carbon capture and subsurface storage [14, 15].

* Correspondence: yuhe.wang@tamu.edu

** Part of this work was conducted by the first and second authors at Texas A&M University's Qatar branch campus.

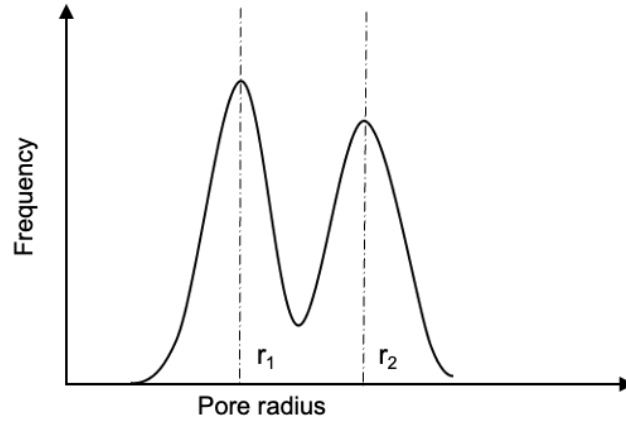


Figure 1. An illustration of a typical bimodal pore size distribution

The bimodal porous structure leads to bimodal permeabilities in the microporous and microporous system [16]. If we decompose the porous bulk into two portions – microporous and microporous portion, the permeability of the microporous portion is often in a few hundreds of milli-Darcy, while the microporous portion often exhibits permeability in just a few milli-Darcy [17]. This results in a distinct difference in the flow capacity or conductivity of the two systems. In a typical porous medium, the pore space formed by solid grains facilitates flow conductivity. However, in microporous carbonates, the grains are filled with micropores rather than being absolute solid, a feature linked to their geological origins and observed by computed tomography imaging of rock samples [18, 19, 20, 21].

To understand the fluid flow phenomena in a bimodal porous medium like the microporous carbonates, it is evident that one cannot simply ignore the large portion of micropores. The significant pore size discrepancy introduces substantial computational challenges. At a scale where detailed macropores can be resolved, one can relatively easily solve the Stokes flow through the microporous portion if the contribution of micropores in grains is ignored. However, to account for the micropores, it would be necessary to zoom in on every grain to resolve these micropores and solve a coupled system, which could present enormous difficulties at the boundary between macropores and micropores. Even if one were able to overcome the challenges of modeling the detailed fluid flow in a zoom-in region of microporous carbonates, it would still be impossible to capture the full spectrum of pore-scale configurations of a macroscale system, even with the most advanced tomography technology. The level of detail in imaging is inversely proportional to the sampling size, resulting in extremely sparse and incomplete information on a macroscale system.

Microscale imaging, dynamic imaging, and modeling provide a viable approach for obtaining direct information at microscale or pore scale. However, it is essential to understand how to scale these microscale results to the macroscale. Detailed microscale modeling of fluid flow may be of little value if scaled learning or mean characteristics of the media and flow cannot be extracted. Therefore, the concept of physical similarity or scaled learning should not be overlooked in the pursuit of microscale modeling. Indeed, the theory of fluid flow has evolved and should continue to evolve toward obtaining the mean characteristics of the media and flow, and formulating the basic laws based on these mean characteristics. Whether in regular or microporous systems, this approach is important toward understanding and modeling fluid flow in porous media.

In pursuit of these mean characteristics and scaling laws for physical similarity, we work on a simple mathematical model in this part to describe the fluid flow process through bimodal porous media. We discuss the basic laws and introduce the mean characteristics derived from the mathematical model. This work in modeling fluid flow through bimodal porous media is to assist our understanding of fluid mechanics in such media and have many implications in various scientific and engineering applications as discussed above.

In this part, we present a mathematical model based on the assumption of a specific microporous structure. We outline the basic concepts of the model. We demonstrate the journey to the self-similar solution. We present and discuss the mathematical equations and the solution characteristics.

Basic model. We start by introducing a heuristic model for fluid flow through bimodal porous media. This model is based on pore-scale tomography images. Figure 2 shows a conceptual illustration of bimodal porous media at the pore scale. We assume the porous space is divided into two portions: one representing macropores and another consisting of inclusions with micropores. These microporous inclusions simplify the concept of microporous grains. In microporous carbonates, macropores have a pore size of a few hundred microns with permeability around a few hundred milli-Darcy. Micropores, on the other hand, have a pore size of a few microns with permeability around a few milli-Darcy.

In this basic model, we refer to the microporous continuum as the primary medium and the microporous inclusions as the secondary medium (**Figure 2**). Inspired by the pioneering work on fluid flow in fissured rocks [23], we develop a double-continuum model for porous media with microporous inclusions. At this stage, the model operates at the pore scale or microscale. Given the low Reynolds number, it is reasonable to assume that flow in the primary medium follows Stokes flow.

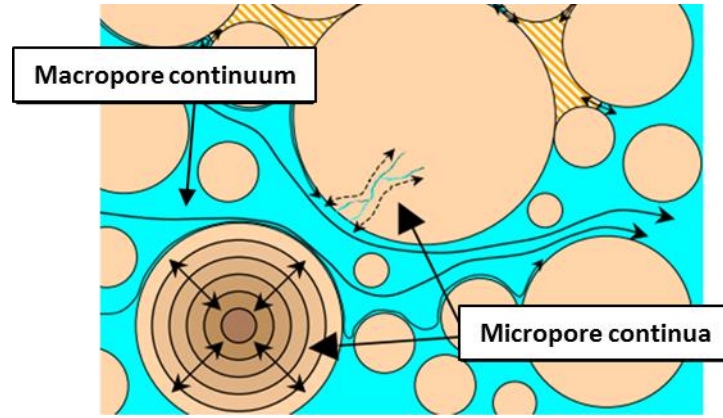


Figure 2. An illustration of a typical microporous example, adopted from [22]

The basic model introduces two fluid pressures at the same spatial point: one for the primary medium and one for the secondary medium. We also account for the transfer between these two media. While the basic model has a heuristic foundation, the subsequent analysis is rigorous. This heuristic approach includes several key points essential for understanding the rigorous analysis and solutions that follow.

Double-continuum model equations. Based on mass conservation, we can write two equations: one for the primary medium and another for the secondary medium.

$$\frac{\partial(\phi_1 \rho)}{\partial t} + \text{div}(\rho u) = \rho \sigma \frac{k_s}{\mu} (p_2 - p_1) \quad (1)$$

$$\frac{\partial(\phi_2 \rho)}{\partial t} = \rho \sigma \frac{k_s}{\mu} (p_1 - p_2) \quad (2)$$

where ρ is the fluid density, ϕ_1 and ϕ_2 are the porosities of the primary and secondary medium, u is the fluid velocity, σ is a factor characterizing the geometry of the bimodal porous media, k_s is a permeability relating to the transfer capability between the two media, μ is the fluid viscosity, p_1 and p_2 are the fluid pressures of the primary and secondary medium. The flow in the primary medium at pore scale is assumed to follow Stokes, such that we have

$$-2\mu \nabla \cdot Du + \nabla p_1 = 0 \quad (3)$$

Due to the low permeability of the secondary medium and its representation as microporous inclusions, we disregard the flow within the secondary medium itself. It only contributes to the flow in the primary medium in a slow and steady-state manner. This basic mathematic model has several interesting aspects. Notably, the assumption implies

that a spatial point in the secondary medium connects only with the corresponding point in the primary medium, with no connections defined within the secondary medium.

Rewriting in terms of fluid pressure p_1 and p_2 , we have

$$\phi_1 c_1 \frac{\partial p_1}{\partial t} + \text{div}(u) = \sigma \frac{k_s}{\mu} (p_2 - p_1) \quad (4)$$

$$\phi_2 c_2 \frac{\partial p_2}{\partial t} = \sigma \frac{k_s}{\mu} (p_1 - p_2) \quad (5)$$

where c_1 and c_2 are the compressibility of the primary and secondary medium.

We then can combine **Equation (4)** and **(5)** to eliminate p_2 ,

$$\frac{\mu}{\sigma k_s} \phi_1 c_1 \phi_2 c_2 \frac{\partial^2 p_1}{\partial t^2} + (\phi_1 c_1 + \phi_2 c_2) \frac{\partial p_1}{\partial t} + \text{div} \left(u + \frac{\mu}{\sigma k_s} \phi_2 c_2 \frac{\partial u}{\partial t} \right) = 0 \quad (6)$$

At the first glance, one can see the similarity between **Equation (6)** and the governing equation for ordinary porous media flow. We can interpret **Equation (6)** as an apparent mass balance equation for flow in bimodal porous media. Additionally, we can define an apparent velocity, which is:

$$u_a = u + \frac{\mu}{\sigma k_s} \phi_2 c_2 \frac{\partial u}{\partial t} \quad (7)$$

It should be noted that σ carries the geometrical characteristics of the bimodal media and is inversely proportional to l^2 , where l is the characteristic length or size of the secondary medium. σk_s characterizes the intensity of fluid transfer between the secondary and primary media, depending on the permeability of the microporous inclusion and the extent of inclusion in the bimodal media. One can think of σ as a measure of the specific surface area of the contact between pore and microporous inclusion. As σ approaches infinity, it corresponds to a reduction in the dimension of the secondary medium and an increase in the portion of the primary media. **Equation (6)** then tends to coincide with the ordinary equation for fluid flow in porous media, and the apparent velocity approaches the true velocity.

Properties of the basic model. The double-continuum model exhibits peculiar features due to the nature of the system described by **Equation (4)** and **(5)**. These uncommon features relate to a medium that contains inclusions with relatively negligible permeability but a large storage volume. To understand this, we first analyze its boundary value properties. In the context of fluid flow, a homogenous initial condition is of primary interest. Our analysis focuses on two key types of boundary conditions: Dirichlet and Neumann. We further narrow the discussion to a case of particular engineering interest, where the initial and boundary conditions are unrelated. One can observe a peculiar behavior in the existence of boundary discontinuities in pressure p_1 and the first-order spatial derivative of p_1 , which cannot be eliminated instantaneously. This is a distinct characteristic of the double-continuum model compared to the ordinary porous media flow model.

Discontinuities of boundary value. Considering a surface at $x = 0$, let's examine the one-dimensional case with a sufficiently small vicinity $S = (-h \leq x \leq h, 0 \leq t \leq T)$ on both sides of this surface. The variable x follows the normal direction to this surface. h is a small quantity and T represents an arbitrary time. We simplify our analysis by applying the Hagen-Poiseuille equation $u = -\frac{R^2}{8\mu} \frac{\partial p_1}{\partial x}$ to describe the Newtonian laminar flow crossing this surface [24, 25]. R is the radius of the 1D flow in dimension perpendicular to x . With these considerations, we can write **Equation (6)** as:

$$Lp_1 := \alpha_1 \frac{\partial^2 p_1}{\partial t^2} + \alpha_2 \frac{\partial p_1}{\partial t} - \beta_1 \frac{\partial^2 p_1}{\partial x^2} - \beta_2 \frac{\partial^3 p_1}{\partial x^2 \partial t} = 0 \quad (8)$$

where $\alpha_1 = \frac{\mu}{\sigma k_s} \phi_1 c_1 \phi_2 c_2$, $\alpha_2 = \phi_1 c_1 + \phi_2 c_2$, $\beta_1 = \frac{R^2}{8\mu}$, and $\beta_2 = \frac{\phi_2 c_2 R^2}{8\sigma k_s}$.

We further assume that p_1 is continuous to satisfy **Equation (8)**. By applying integration by parts, we obtain:

$$[p_1] = [p_1]_{t=0} e^{-\beta_1 t / \beta_2} \quad (9)$$

$$\left[\frac{\partial p_1}{\partial x} \right] = \left[\frac{\partial p_1}{\partial x} \right]_{t=0} e^{-\beta_1 t / \beta_2} \quad (10)$$

where $[\cdot]$ denotes the difference between the values on both sides of the discontinuity surface. The derivations of **Equation (9)** and **(10)** is to be provided in Part 2 of this note.

In its physical sense, the jump in pressure as indicated by **Equation (9)** and the jump in the normal derivative of pressure as shown in **Equation (10)**, caused by the discontinuities or inconsistent initial conditions, decay according to the law $e^{-\beta_1 t / \beta_2}$ rather than being eliminated instantaneously, as in an ordinary porous medium. One also should note that the normal derivative of pressure is proportional to fluid velocity u . We denote this property is a characteristic of the mathematical description of fluid flow in bimodal porous media. The jump tends to disappear as time approaches infinity for bimodal porous media. For a fixed time, one can observe that this jump also tends to vanish as σ goes to infinity. Indeed, in the limiting case where σ is infinity, bimodal porous media behave like ordinary porous media. This is an important property of this boundary value problem. Although there is a jump in velocity at the boundary, the total flow, or apparent velocity, remains continuous. This finding is critical when seeking solutions under constant velocity condition. This property suggests that one should use the apparent velocity to impose the boundary velocity condition.

Solution Characteristics. We then seek to determine the solution characteristics of the model equation, **Equation (8)**, under the following conditions:

$$\begin{aligned} p_1(x, 0) &= p_0, & 0 \leq x < \infty \\ p_1(0^-, t) &= p_b \\ p_1(\infty, t) &= p_0 \end{aligned} \quad (11)$$

Equation (11) says, at the initial instant, there is a fluid pressure change of $(p_0 - p_b)$ at the boundary. The fluid pressure immediately to the right of the boundary equal to $p(0^+, t) = p_b + (p_0 - p_b)e^{-\sigma/\tau t}$. To find the pressure distribution at any instant of time t , we let $h(x, t) = \frac{p_0 - p_1(x, t)}{p_0 - p_b}$ where $h(x, t)$ satisfies:

$$\begin{aligned} \alpha_1 \frac{\partial^2 h}{\partial t^2} + \alpha_2 \frac{\partial h}{\partial t} - \beta_1 \frac{\partial^2 h}{\partial x^2} - \beta_2 \frac{\partial^3 h}{\partial x^2 \partial t} &= 0, & 0 \leq x < \infty, \quad t > 0 \\ h(x, 0) &= 0, & 0 \leq x < \infty \\ h(0^+, t) &= 1 + e^{-\frac{\beta_1}{\beta_2} t}, & t > 0 \\ h(\infty, 0) &= 0 \end{aligned} \quad (12)$$

Applying Laplace transformation and residue theorem, we obtain:

$$h(x, t) = 1 - \frac{1}{\pi} \int_0^1 e^{-\frac{\beta_1}{\beta_2} t} \sin \left(\sqrt{\frac{\lambda(1-c\lambda)}{1-\lambda}} \sqrt{\frac{\alpha_2}{\beta_2}} x \right) \frac{d\lambda}{\lambda(1-\lambda)} \quad (13)$$

where $c = \frac{\alpha_1 \beta_1}{\alpha_2 \beta_2}$.

Let $z = \frac{\beta_1}{\beta_2} t$ and $\xi = \sqrt{\frac{\alpha_2}{\beta_1}} \frac{x}{\sqrt{t}}$, we arrive at its self-similar solution in terms of

$$h(x, t) \Rightarrow h(\xi) = 1 - \frac{1}{\pi} \int_0^1 e^{-z\lambda} \sin \left(\sqrt{\frac{\lambda(1-c\lambda)}{1-\lambda}} \xi \sqrt{z} \right) \frac{d\lambda}{\lambda(1-\lambda)} \quad (14)$$

We can further change the integration limit from $[0, 1]$ to $[0, \infty]$ as shown in

$$h(x, t) = 1 - \frac{1}{\pi} \int_0^\infty e^{-\frac{\beta_1 v^2}{\alpha_2 + \beta_2 v^2} t} \sin \left(v x \sqrt{\frac{\alpha_2 + \beta_2(1-c)v^2}{\alpha_2 + \beta_2 v^2}} \right) \frac{2dv}{v} \quad (15)$$

Let $\xi = \frac{x}{2\sqrt{\beta_1 t / \alpha_2}}$, we can have $4\xi^2 = \frac{\alpha_2 x}{\beta_1 t}$. Then,

Equation (15) becomes:

$$h(\xi) = 1 - \frac{1}{\pi} \int_0^\infty e^{-\frac{v^2}{4\xi^2 + \frac{\beta_2}{\beta_1}} t} \sin \left(v \sqrt{\frac{4\xi^2 \beta_1 t + \beta_2(1-c)v^2}{4\xi^2 \beta_1 t + \beta_2 v^2}} \right) \frac{2dv}{v} \quad (16)$$

Since $\beta_2 = \frac{\phi_2 c_2 R^2}{8\sigma k_s} \propto \frac{1}{\sigma}$, we can see β_2 tends to 0 as σ approaches to infinity, which clearly corresponds to a dimension reduction of the secondary medium and an increase of the portion of the primary medium. When $\beta_2 \rightarrow 0$, **Equation (13)** becomes:

$$h(x, t) = 1 - \frac{2}{\pi} \int_0^\infty e^{-\frac{\beta_1}{\alpha_2} v^2 t} \sin(vx) \frac{dv}{v} \quad (17)$$

If we then let $u = vx$ and $\xi = \frac{x}{2\sqrt{(\beta_1/\alpha_2)t}}$, **Equation (17)** can be written as:

$$h(x, t) = 1 - \frac{2}{\pi} \int_0^\infty e^{-\frac{u^2}{4\xi^2}} \frac{\sin u}{u} du \quad (18)$$

Note that in **Equation (15)** we apply the same self-similar variable ξ up to a scaling scalar. The well-known self-similar solution of classical porous media flow equation is obtained from **Equation (16)**. In the error function form, we have

$$\begin{aligned} h(x, t) &= 1 - \frac{2}{\pi} \operatorname{erf}(\xi) \\ \text{or} \\ p_1(x, t) &= p_b + \frac{2}{\pi} (p_0 - p_b) \operatorname{erf}(\xi) \end{aligned} \quad (19)$$

Concluding remarks. In Part 1, we provide a simple mathematical model for fluid flow in bimodal porous media. We demonstrate the process of reaching a self-similar solution at microscale. We discuss the discontinuities of the boundary value and the solution characteristics, which could provide valuable insights. When dealing fluid flow processes in bimodal porous media, the ordinary equations of porous media flow can be applied only if the characteristic times of the process under consideration are long compared to the delay time. However, if it is not the case, the basic dual-continuum model presented in this note may be necessary. In many instances, it is crucial to consider the secondary pores when investigating such processes. In the next part of this study, we provide the homogenization of the basic model to Darcy scale in the classic pressure transient analysis context of petroleum reservoir studies. We also discuss previously unrevealed flow behaviors and the related engineering implications.

Some intermediate steps in the derivation of the solutions have been omitted. For those details, please contact the corresponding author.

References

1. Song, Y.Q., Ryu, S. and Sen, P.N., 2000. Determining multiple length scales in rocks. *Nature*, 406(6792), pp.178-181.
2. Wang, M., Cheung, S.W., Chung, E.T., Vasilyeva, M. and Wang, Y., 2020. Generalized multiscale multicontinuum model for fractured vuggy carbonate reservoirs. *Journal of Computational and Applied Mathematics*, 366, p.112370.
3. Mi, L., Yan, B., Jiang, H., An, C., Wang, Y. and Killough, J., 2017. An Enhanced Discrete Fracture Network model to simulate complex fracture distribution. *Journal of Petroleum Science and Engineering*, 156, pp.484-496.
4. Yan, B., Mi, L., Chai, Z., Wang, Y. and Killough, J.E., 2018. An enhanced discrete fracture network model for multiphase flow in fractured reservoirs. *Journal of Petroleum Science and Engineering*, 161, pp.667-682.
5. Na, K., Jo, C., Kim, J., Cho, K., Jung, J., Seo, Y., Messinger, R.J., Chmelka, B.F. and Ryoo, R., 2011. Directing zeolite structures into hierarchically nanoporous architectures. *Science*, 333(6040), pp.328-332.
6. Lee, P.F., Zhang, X., Sun, D.D., Du, J. and Leckie, J.O., 2008. Synthesis of bimodal porous structured TiO₂ microspheres with high photocatalytic activity for water treatment. *Colloids and Surfaces A: Physicochemical and Engineering Aspects*, 324(1), pp.202-207.
7. He, G., Ji, X. and Nazar, L., 2011. High “C” rate Li-S cathodes: sulfur imbibed bimodal porous carbons. *Energy & Environmental Science*, 4(8), pp.2878-2883.
8. Moshier, S.O., 1989. Microporosity in micritic limestones: a review. *Sedimentary geology*, 63(3-4), pp.191-

213.

9. Budd, D.A., 1989. Micro-rhombic calcite and microporosity in limestones: a geochemical study of the Lower Cretaceous Thamama Group, UAE. *Sedimentary Geology*, 63(3-4), pp.293-311.
10. Chen, J.S., Li, L., Wang, J.Y., Barry, D.A., Sheng, X.F., Zu Gu, W., Zhao, X. and Chen, L., 2004. Water resources: groundwater maintains dune landscape. *Nature*, 432(7016), pp.459-460.
11. Pak, T., Butler, I.B., Geiger, S., van Dijke, M.I. and Sorbie, K.S., 2015. Droplet fragmentation: 3D imaging of a previously unidentified pore-scale process during multiphase flow in porous media. *Proceedings of the National Academy of Sciences*, 112(7), pp.1947-1952.
12. Zhang, N., Wang, Y., Sun, Q. and Wang, Y., 2018. Multiscale mass transfer coupling of triple-continuum and discrete fractures for flow simulation in fractured vuggy porous media. *International Journal of Heat and Mass Transfer*, 116, pp.484-495.
13. Zhang, F., An, M., Yan, B., Wang, Y. and Han, Y., 2019. A novel hydro-mechanical coupled analysis for the fractured vuggy carbonate reservoirs. *Computers and Geotechnics*, 106, pp.68-82.
14. Lisbona, P., Martínez, A., Lara, Y. and Romeo, L.M., 2009. Integration of carbonate CO₂ capture cycle and coal-fired power plants. A comparative study for different sorbents. *Energy & Fuels*, 24(1), pp.728-736.
15. Falkowski, P., Scholes, R.J., Boyle, E.E.A., Canadell, J., Canfield, D., Elser, J., Gruber, N., Hibbard, K., Höglberg, P., Linder, S. and Mackenzie, F.T., 2000. The global carbon cycle: a test of our knowledge of earth as a system. *science*, 290(5490), pp.291-296.
16. Nelson, P.H., 1994. Permeability-porosity relationships in sedimentary rocks. *The log analyst*, 35(03).
17. Anselmetti, F.S., Luthi, S. and Eberli, G.P., 1998. Quantitative characterization of carbonate pore systems by digital image analysis. *AAPG bulletin*, 82(10), pp.1815-1836.
18. Remeysen, K. and Swennen, R., 2008. Application of microfocus computed tomography in carbonate reservoir characterization: possibilities and limitations. *Marine and Petroleum Geology*, 25(6), pp.486-499.
19. Sok, R.M., Knackstedt, M.A., Varslot, T., Ghous, A., Latham, S. and Sheppard, A.P., 2010. Pore scale characterization of carbonates at multiple scales: Integration of Micro-CT, BSEM, and FIBSEM. *Petrophysics*, 51(06).
20. Santini, M., Marzorati, S., Fest-Santini, S., Trasatti, S. and Cristiani, P., 2017. Carbonate scale deactivating the biocathode in a microbial fuel cell. *Journal of Power Sources*.
21. Norbistrath, J.H., Eberli, G.P., Laurich, B., Desbois, G., Weger, R.J. and Urai, J.L., 2015. Electrical and fluid flow properties of carbonate microporosity types from multiscale digital image analysis and mercury injection. *AAPG Bulletin*, 99(11), pp.2077-2098.
22. Lichtner, P., Kang, Q., 2006. Role of pore-scale heterogeneity on reactive flows in porous materials: validity of the continuum representation of reactive transport. In *XVI International Conference on Computational Methods in Water Resources (CMWRXVI)*
23. Barenblatt, G.I., Zheltov, I.P. and Kochina, I.N., 1960. Basic concepts in the theory of seepage of homogeneous liquids in fissured rocks [strata]. *Journal of applied mathematics and mechanics*, 24(5), pp.1286-1303.
24. Wu, K., Chen, Z., Li, J., Li, X., Xu, J. and Dong, X., 2017. Wettability effect on nanoconfined water flow. *Proceedings of the National Academy of Sciences*, 114(13), pp.3358-3363.
25. Song, H., 2018. *Engineering fluid mechanics* (Vol. 2024). Singapore: Springer.